Different stages of flame acceleration from slow burning to Chapman-Jouguet deflagration

Damir M. Valiev,[1,2] Vitaly Bychkov,[1] V'yacheslav Akkerman,[1,3] and Lars-Erik Eriksson[4]
[1]*Department of Physics, Umeå University, S-901 87 Umeå, Sweden*
[2]*Department of Materials Science and Engineering, Royal Institute of Technology, SE-10044 Stockholm, Sweden*
[3]*Department of Mechanical and Aerospace Engineering, Princeton University, D323-A, Engineering Quad., Princeton, New Jersey 08544-5263, USA*
[4]*Department of Applied Mechanics, Chalmers University of Technology, 412 96 Göteborg, Sweden*
(Received 28 August 2008; revised manuscript received 4 June 2009; published 29 September 2009)

Numerical simulations of spontaneous flame acceleration are performed within the problem of flame transition to detonation in two-dimensional channels. The acceleration is studied in the extremely wide range of flame front velocity changing by 3 orders of magnitude during the process. Flame accelerates from realistically small initial velocity (with Mach number about 10^{-3}) to supersonic speed in the reference frame of the tube walls. It is shown that flame acceleration undergoes three distinctive stages: (1) initial exponential acceleration in the quasi-isobaric regime, (2) almost linear increase in the flame speed to supersonic values, and (3) saturation to a stationary high-speed deflagration velocity. The saturation velocity of deflagration may be correlated with the Chapman-Jouguet deflagration speed. The acceleration develops according to the Shelkin mechanism. Results on the exponential flame acceleration agree well with previous theoretical and numerical studies. The saturation velocity is in line with previous experimental results. Transition of flame acceleration regime from the exponential to the linear one, and then to the constant velocity, happens because of gas compression both ahead and behind the flame front.

DOI: 10.1103/PhysRevE.80.036317 PACS number(s): 47.70.Pq, 47.20.Ma, 47.27.Cn

I. INTRODUCTION

For a long time, deflagration-to-detonation transition (DDT) was one of the least understood processes in hydrodynamics, nonlinear physics, combustion science and astrophysics in spite of its extreme importance. During the DDT process a usual slow flame accelerates spontaneously with velocity increase by 3 orders of magnitude until an explosion happens and develops into a self-sustained detonation [1–10]. In the present work we study the stage of flame acceleration, which is the initial and essential part of DDT in tubes. The first qualitative explanation of the flame acceleration has been suggested by Shelkin in the 1940s [1,2]. The Shelkin mechanism involved thermal expansion of the burning gas, nonslip at the tube walls and turbulence as the main components of flame acceleration. When a flame propagates from a closed tube end, burning gas expands and pushes a flow of the fuel mixture. The flow becomes strongly nonuniform because of nonslip at the walls. The nonuniform velocity distribution makes the flame shape curved, which increases the burning rate and drives the acceleration. Turbulence provides additional distortion of the flame front and compensates for thermal losses to the walls. Acceleration of turbulent flames was observed in numerous experiments [3–10], still, for a long time there was almost no progress in the quantitative theoretical understanding of the process because of the complications related to turbulent burning. Despite a century of intensive research, turbulence in general and turbulent burning in particular belong to the most difficult problems of modern physics [11–17].

Considerable progress in understanding the flame acceleration started recently with the numerical simulations and the analytical theory supporting each other. The numerical simulations [18,19] demonstrated the possibility of a laminar flame acceleration and the DDT in channels with adiabatic walls. The analytical theory of laminar flame acceleration in smooth tubes has been developed and validated by extensive numerical simulations in Refs. [20–22]. The theory of flame acceleration [20–22] employed the limit of an incompressible flow, which holds with a good accuracy at the beginning of the process. For example, a typical value of the laminar flame velocity U_f for hydrocarbon flames is about 40 cm/s, which is much smaller than the sound speed c_s in the fuel mixture. Initial values of the Mach number are of the order of $\mathrm{Ma} \equiv U_f / c_s = 10^{-3}$, therefore effects of adiabatic gas compression may be neglected at the beginning of flame acceleration. The theory [20,21] predicted fast acceleration of laminar flames in microscale tubes. Recent experiments on the DDT in ethylene-oxygen mixtures confirmed the theoretical predictions for tubes with diameters about 1 mm [23]. However, the numerical simulations of Refs. [18,24] obtained a much slower regime of flame acceleration in comparison with the exponential one found in Refs. [19–21], see also the discussion in Ref. [25]. The exponential regime was missed out in Refs. [18,24], because these papers employed relatively high initial values of the Mach number (about 0.05). High initial values of the Mach number are not quite realistic; still, they are often used in the simulations of the DDT to avoid difficulties related to extremely wide range in the length scales and flame front velocities. By assuming high initial values of the Mach number, a researcher reduces the computational time of the DDT modeling considerably, but loses the details of the flame acceleration process. For example, in Refs. [18,24], the flame front velocity increased only by order of magnitude before the explosion, instead of 3 orders of magnitude needed for a slow flame to accelerate to supersonic speed. Taking an artificially high initial Mach number may lead to an erroneous conclusion that DDT is possible without flame acceleration, or to obscure the role of

flame acceleration. We stress that flame acceleration is a key process in DDT in tubes. So far there were no attempts to trace the whole process of flame acceleration in the DDT in detail for realistically small initial Mach numbers. There was no systematic investigation of flame acceleration at large values of the Mach number either. Such a task was performed only for the quasi-isobaric regime of flame acceleration at the very beginning of the process [20–22]. This created a large gap between the theory and the experiments on the DDT. For example, the experiments [23] demonstrated that flame acceleration may saturate to a stationary velocity below the Chapman-Jouguet (CJ) detonation speed. The saturation velocity may be interpreted as the CJ deflagration speed [26,27], which is subsonic with respect to the fuel mixture just ahead of the flame front and supersonic in the reference frame of the tube walls. Similar saturation of the flame propagation speed to a supersonic value with respect to an observer has been detected experimentally in channels with obstacles; this regime is often called "fast flames" [10,28]. The theory and simulations [20,21] did not reproduce any of these effects, even qualitatively. So, there has been a crucial controversy between different results on flame acceleration in DDT, which had to be resolved.

The purpose of the present work is to investigate systematically the flame acceleration in the extremely wide range of Mach numbers changing by 3 orders of magnitude during the DDT. We perform numerical simulations of flame acceleration in tubes with smooth nonslip adiabatic walls. The simulations are performed in the two-dimensional (2D) planar geometry. Flame accelerates from realistically small initial velocity with Mach number 10^{-3} to supersonic speed in the reference frame of the tube walls. We show that flame acceleration undergoes three distinctive stages: (1) initial exponential acceleration in the quasi-isobaric regime similar to the previous works [20,21]; (2) linear increase in the flame velocity to supersonic speed with almost constant acceleration; (3) saturation to a stationary high-speed deflagration velocity. The saturation velocity may be correlated with the CJ deflagration speed. The acceleration develops according to the Shelkin mechanism. Results on the exponential flame acceleration agree well with the previous theoretical and numerical studies [20,21]. The saturation velocity is qualitatively in line with previous experimental results [10,23,28]. Transition of flame acceleration regime from the exponential to the linear one, and then to the constant velocity, happens because of gas compression both ahead and behind the flame front.

II. BASIC EQUATIONS, BOUNDARY AND INITIAL CONDITIONS, AND PHYSICAL PARAMETERS

We performed numerical simulations of the 2D planar hydrodynamic combustion equations including transport processes and chemical kinetics

$$\frac{\partial \rho}{\partial t} + \frac{\partial}{\partial x_i}(\rho u_i) = 0, \tag{1}$$

$$\frac{\partial}{\partial t}(\rho u_i) + \frac{\partial}{\partial x_j}(\rho u_i u_j + \delta_{ij} p - \zeta_{ij}) = 0, \tag{2}$$

$$\frac{\partial}{\partial t}\left(\rho \varepsilon + \frac{1}{2}\rho u_i u_i\right) + \frac{\partial}{\partial x_j}\left(\rho u_j h + \frac{1}{2}\rho u_i u_i u_j + q_j - u_i \zeta_{ij}\right) = 0, \tag{3}$$

$$\frac{\partial}{\partial t}(\rho Y) + \frac{\partial}{\partial x_i}\left(\rho u_i Y - \frac{\mu}{\mathrm{Sc}}\frac{\partial Y}{\partial x_i}\right) = -\frac{\rho Y}{\tau_R}\exp(-E/R_p T), \tag{4}$$

where Y is the mass fraction of the fuel mixture, $\varepsilon = QY + C_V T$ is the internal energy, $h = QY + C_p T$ is the enthalpy, Q is the energy release in the reaction, C_V, C_p are the heat capacities at constant volume and pressure. We take $C_V = 5R_p/2m$, $C_p = 7R_p/2m$, where $R_p \approx 8.31$ J/(mol·K) is the perfect gas constant. We consider a single irreversible Arrhenius reaction of the first order with the activation energy E and the constant of time dimension τ_R. The stress tensor ζ_{ij} and the energy diffusion vector q_j are

$$\zeta_{ij} = \mu\left(\frac{\partial u_i}{\partial x_j} + \frac{\partial u_j}{\partial x_i} - \frac{2}{3}\frac{\partial u_k}{\partial x_k}\delta_{ij}\right), \tag{5}$$

$$q_j = -\mu\left(\frac{C_p}{\mathrm{Pr}}\frac{\partial T}{\partial x_j} + \frac{Q}{\mathrm{Sc}}\frac{\partial Y}{\partial x_j}\right), \tag{6}$$

where $\mu \equiv \rho\nu$ is the dynamic viscosity, Pr and Sc are the Prandtl and Schmidt numbers, respectively. The gas mixture is a perfect gas with the equation of state $P = \rho R_p T/m$ and a constant molecular weight $m = 2.9 \times 10^{-2}$ kg/mol. The adiabatic exponent of the gas was $\gamma = 1.4$. We consider a flame propagating in a 2D tube of half-width R with nonslip conditions at the adiabatic walls. The flame propagates from the closed end of the tube to the open one. We take the initial pressure and temperature of the fuel mixture $P_f = 10^5$ Pa and $T = 300$ K, respectively. The thermal and chemical parameters of the fuel mixture were chosen to reproduce the most important properties of methane and propane laboratory flames. We took the planar flame velocity $U_f = 0.347$ m/s with the initial Mach number $\mathrm{Ma} = U_f/c_s = 10^{-3}$. The flame thickness in our calculations is defined conventionally as $L_f \equiv \nu/\mathrm{Pr}\, U_f$. Still, the effective flame thickness is considerably larger, see [24]. Thermal expansion at the planar flame front $\Theta = \rho_f/\rho_b$ is determined by the energy release in the reaction; we took $\Theta = 8$ typical for methane and propane burning. We use the dynamic viscosity $\mu = 1.7 \times 10^{-5}$ Ns/m^2 with the Prandtl number Pr = 0.75. To avoid the Zeldovich (thermal-diffusion) instability we take unit Lewis number $\mathrm{Le} \equiv \mathrm{Pr}/\mathrm{Sc} = 1$. The activation energy was $E = 32R_p T_f$.

In the present simulations we considered different tube widths $10L_f < 2R < 30L_f$. For typical hydrocarbon-air flames this corresponds to the tube diameters (widths) roughly between 0.6 to 2 mm. Though being small, these values are comparable to the tube diameters used in the DDT experiments [23]. Presumably, heat loss to the walls plays a noticeable role in the DDT in narrow tubes. Still, in the present paper we study only the case of adiabatic walls.

Similar to our previous papers [20–22], we used the Zeldovich-Frank-Kamenetsky solution for a planar flame front as an initial condition. The planar flame front was created at a distance $4L_f$ from the closed tube end. We kept

nonreflecting boundary conditions at the open end of the tube, though normally shock waves cannot reach open end due to adaptive mesh refinement. One of the main dimensionless parameters of the problem is defined as $\mathrm{Re}=RU_f/\nu$, and it plays the role of the initial Reynolds number related to the flame dynamics. Taking into account the formula for the flame thickness L_f, we couple the Reynolds number to the scaled tube half-width as $\mathrm{Re}=R/\mathrm{Pr}\,L_f$. By changing the tube half-width R we varied the Reynolds number. We stress that the traditional Reynolds number describing the flow, $\mathrm{Re}_{flow}=2\langle u\rangle R/\nu$, is different from the present definition $\mathrm{Re}=RU_f/\nu$. Here, $\langle u\rangle$ is the flow velocity averaged over the cross-section. In our simulations the value Re_{flow} was as large as 10^4 and above at the end of the acceleration process, which produced noticeable turbulence at the explosion stage of the DDT. Still, no turbulence was detected during the flame acceleration. We mark that turbulence in a tube flow with stationary boundary conditions (the Poiseuille flow) develops for $\mathrm{Re}_{flow}>(2-3)\cdot 10^3$. Thus, the present values of the Reynolds number are not so large, taking into account that the flow produced by an accelerating flame is nonstationary. One may also expect difficulties with resolution of the boundary layer at such values of the Reynolds number. However, here we stress that the boundary layer ahead of an accelerating flame is quite different from the classical boundary layer produced by a stationary flow. In the classical case, thickness of the boundary layer decreases with increase in the flow velocity (of the Reynolds number) as $\propto 1/\sqrt{\langle u\rangle}$. On the contrary, the theory and modeling of [20,21] indicate that thickness of the boundary layer generated by an accelerating flame is about R/Θ independent of the Reynolds number, which may be resolved quite well with the used mesh. Our present simulations confirm the theoretical estimates, see Appendix.

III. RESULTS AND DISCUSSION

The purpose of the present paper is to study flame acceleration in DDT starting with the realistically small initial Mach number $\mathrm{Ma}=U_f/c_s=10^{-3}$ and finishing with supersonic final velocities of the reaction front. We started with a probe simulation run taking a small value of the Reynolds number Re=6.67 (corresponding to the tube width $10L_f$). Figure 1 presents tip velocity of the reaction front versus time obtained in the simulation run. The plot demonstrates (at least qualitatively) all elements of the DDT as described in the Shelkin scenario. First, the flame front accelerates from very low subsonic velocities to supersonic speed in the laboratory reference frame with respect to the tube walls. Then, we observe an abrupt explosion leading to strong increase in the reaction speed. Finally, the explosion develops into detonation. Figure 1 gives the idea of the whole process of DDT. However, in the present work we are interested only in the first part of the process, namely, in the flame acceleration. The reasons for such limitation are both numerical and methodological as explained in the Appendix. The dashed vertical line in Fig. 1 indicates the range of the present numerical quantitative study. The details of the explosion process that starts after the designated moment are mostly beyond the scope of the present work.

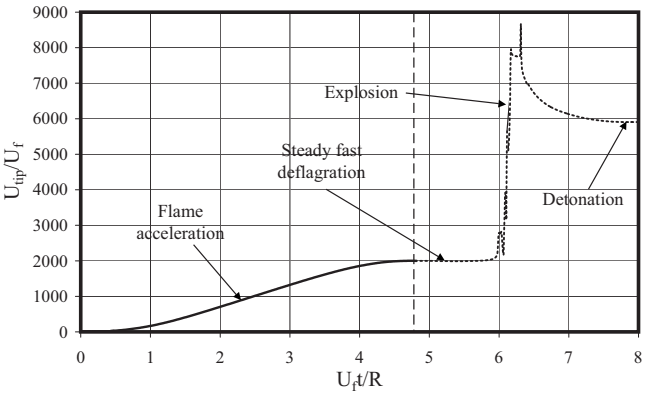

FIG. 1. Time dependence of scaled velocity U_{tip}/U_f for Re =6.67 is shown until full-developed CJ detonation. The dashed vertical line indicates that the range of the quantitative study is limited by the moment of explosion onset.

Focusing at the process of flame acceleration, we observe several different stages of the process described below. At the beginning, the flame accelerates exponentially from realistically small velocities with low initial value of the Mach number $\mathrm{Ma}=U_f/c_s=10^{-3}$ typical for hydrocarbon flames. At the end of the acceleration, we obtained supersonic velocities of the complex of a curved flame front and shocks in the laboratory reference frame. For comparison, the analytical theory and numerical simulations of [20,21] considered only early stages of flame acceleration with the burning rate increasing approximately 10 times in comparison with the planar flame velocity. On the contrary, papers [18,24] studied in detail only final stages of the DDT taking an artificially large initial Mach number. Here we investigate in detail all stages of the flame acceleration. We performed simulations for four values of the Reynolds number within the limits $6.67<\mathrm{Re}=R/\mathrm{Pr}\,L_f<20$ corresponding to the tube widths $10L_f<2R<30L_f$. Figure 2 shows the characteristic shape of an accelerating flame front in a tube with nonslip at the walls: flame propagates to the right; the left end of the tube $z=0$ is closed. For illustrative purposes we used different scales on x and z axes. The flame front is extremely elongated; on this figure it stretches on the distance about $220R$ along the z axis. The physical mechanism of incompressible flame stretching and exponential acceleration in tubes with nonslip walls is described in details in [20,21].

Figure 3 shows the velocity of the flame tip versus time for different tube widths (different values of the Reynolds number). Each velocity graph in Fig. 3 is shown up to the early stage of the explosion onset, covering only the flame

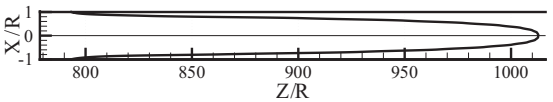

FIG. 2. A flame shape in a tube with nonslip at the walls; Re =6.67, scaled time instant $U_f t/R=4.57$.

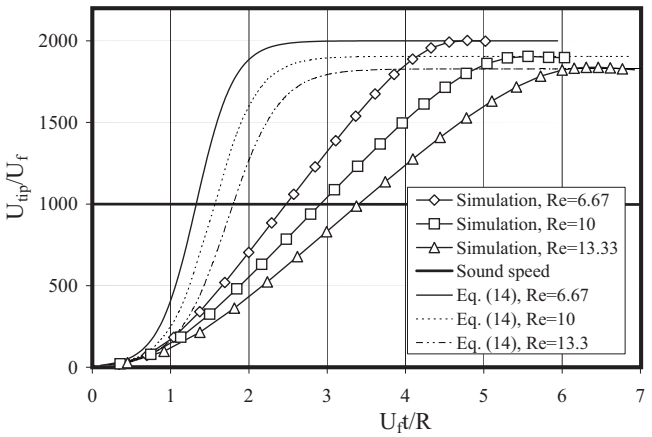

FIG. 3. Time dependence of scaled velocity U_{tip}/U_f for different values of Reynolds number: Re=6.67; 10; 13.3. Each velocity graph is shown until the explosion onset. The lines without markers reproduce the phenomenological formula Eq. (14).

acceleration and velocity saturation stages of the whole DDT process. All plots of the figure demonstrate the same features of flame acceleration. We can recognize three distinctive stages of the flame acceleration in Fig. 3: (1) at the beginning flame accelerates exponentially; (2) then the process slows down to almost constant acceleration; (3) velocity of the flame tip saturates to a stationary supersonic value. The purpose of the present paper is to make a special emphasis on these three stages and to investigate their main features.

At the beginning of the acceleration process, the planar flame starts propagating with velocity ΘU_f with respect to the tube walls. Then we observe exponential acceleration of the flame tip as $U_{tip} \approx \Theta U_f \exp(\sigma U_f t/R)$ in agreement with [20,21]; the analytical formula for the scaled growth rate σ was found in [20,21] as

$$\sigma = \frac{(\mathrm{Re}-1)^2}{4\,\mathrm{Re}}\left(\sqrt{1+\frac{4\,\mathrm{Re}\,\Theta}{(\mathrm{Re}-1)^2}}-1\right)^2. \qquad (7)$$

Our present results agree well with the previous theory and simulations, see Fig. 4. The curve in Fig. 4 corresponds to the analytical formula Eq. (7); empty markers in Fig. 4 show

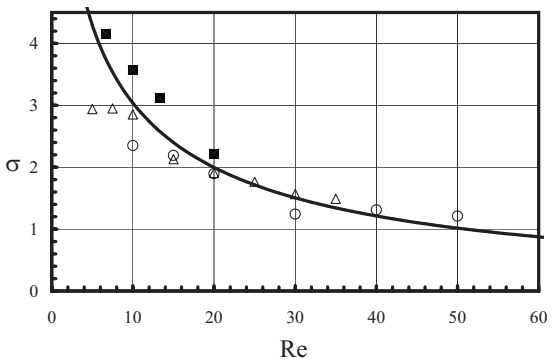

FIG. 4. The acceleration rate σ versus the Reynolds number Re. The solid line presents the theoretical results of Ref. [20]. The empty and the filled markers present the simulation result of Ref. [20] and of the present work, respectively.

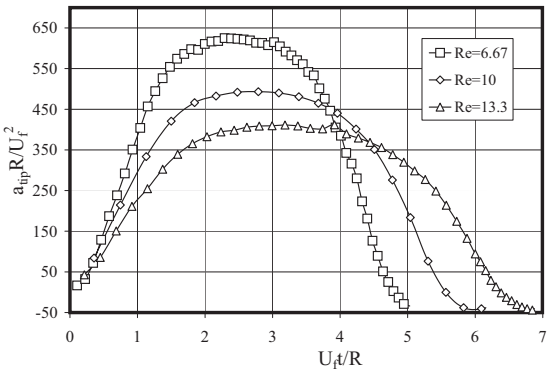

FIG. 5. Time dependence of the scaled acceleration aR/U_f^2.

the numerical results of [20]; the filled markers correspond to the present simulations. In the case of relatively low value of the Reynolds number, Re=6.67, present numerical results agree with the theory even better than the numerical data of [20]. In order to calculate the growth rate σ we considered tip acceleration to the velocities exceeding the initial one by an order of magnitude, about $100U_f$ in the laboratory frame.

Flame accelerates exponentially until the Mach number related to the tip velocity reaches approximately $\mathrm{Ma}_{tip} = U_{tip}/c_s \sim 0.1$ (corresponding to $U_{tip}/U_f \sim 100$ in the present simulations). As the velocity of the flame tip approaches the sound speed, the flow cannot be treated as incompressible any more. Effects of gas compression modify the regime of flame acceleration. Figure 3 demonstrates that the initial exponential regime develops into a different one, which may be described roughly as linear increase in the flame velocity with almost constant acceleration $a = dU_{tip}/dt \approx const$. Time dependence of the scaled acceleration aR/U_f^2 is presented in Fig. 5 for different values of the Reynolds number. All plots of Fig. 5 demonstrate initial exponential growth of the acceleration, which is followed by a rather flat plateau. The plateau corresponds to the regime of almost constant acceleration. Later, the acceleration goes down as the flame velocity saturates.

Figure 6 shows the maximal scaled value of the flame acceleration aR/U_f^2 versus the Reynolds number; the acceleration is quite large for all simulation runs $200 < aR/U_f^2$

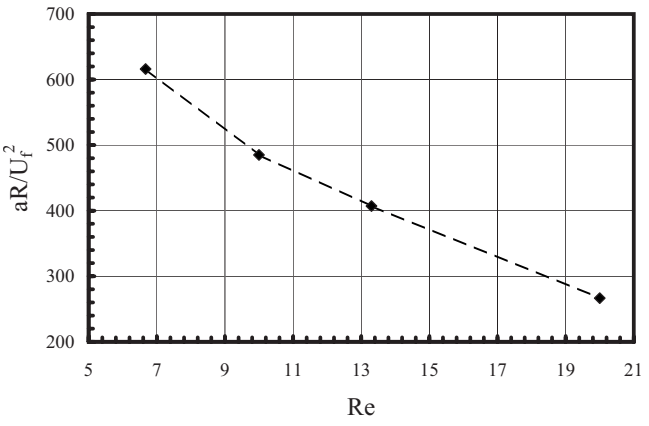

FIG. 6. The scaled acceleration aR/U_f^2 versus the Reynolds number Re.

<700. Similar to the exponential regime, constant acceleration is larger in narrower channels. Transition from the exponential regime to the constant one means slowdown of the flame acceleration process; the slowdown happens because of the gas compression. The physical reason of the slowdown may be understood using the continuity equation, Eq. (1). In the initial incompressible regime of flame acceleration, expanding gas generates a flow mostly in the fresh fuel mixture [20,21]. In order to overcome the viscous force and to drive the flow, the flame has to produce an increased pressure in comparison with the initial one. At small values of the Mach number, relative pressure increase is minor in comparison with the background pressure, and it does not lead to any noticeable compression of the gas. Using Eq. (1), the boundary conditions at the closed tube end, and taking into account almost constant density of the burnt gas, we find that burnt gas remains almost at rest during the initial quasi-isobaric stage of the acceleration. The whole extra volume produced in the burning process goes into the flow of the fuel mixture leading to strong exponential regime of flame acceleration, see the analytical theory [20,21]. The situation changes as the flame accelerates to velocities comparable to the sound speed, i.e., to sufficiently large values of the Mach number $\mathrm{Ma}_{tip}=U_{tip}/c_s$. In that case pressure increase produces considerable adiabatic compression of the gas, both ahead of the flame front and behind the front. Compression of the burnt gas leads to a flow behind the flame front. As a model, we can assume an average one-dimensional (1D) flow of the burnt gas $\mathbf{u}=\hat{\mathbf{e}}_z u_z$ with uniform density depending on time only, $\rho_b=\rho_b(t)$. Solving the continuity equation and taking into account the boundary conditions at the tube end, we find velocity in the burnt gas

$$u_z=-\frac{z}{\rho_b}\frac{d\rho_b}{dt}. \tag{8}$$

Equation (8) predicts a compression flow of the burnt gas in the negative direction, toward the closed tube end. The flow may be rather strong at the back side of the flame front as it moves far from the closed tube end. This flow tends to drift the flame front in the negative direction, i.e., it works against the flame acceleration. The influence of gas compression on flame acceleration has been discussed recently in [29], though in a different context of the DDT in channels with obstacles. Gas compression may be observed directly in Fig. 7 both behind the flame front and ahead of the front. Figure 7 presents density profile along the channel axis at different time instants. Compression of the burnt gas behind the front is relatively uniform in agreement with the above model. On the contrary, in the fresh fuel mixture we can see a nonuniform adiabatic compression wave pushed by the flame. When the flame tip reaches the distance about $Z_{tip}\sim 3\cdot 10^3 R$ from the closed end of the tube, density of the fuel mixture in the compression wave is approximately three to four times larger than the initial value. Maximal possible gas compression in a shock wave may be $(\gamma+1)/(\gamma-1)$, see [26], which equals 6 in the present case. Figure 8 shows scaled distribution of z velocity along the tube axis for the same time instants as Fig. 7. We can see the region of negative velocity behind the flame front, which tends to slow-

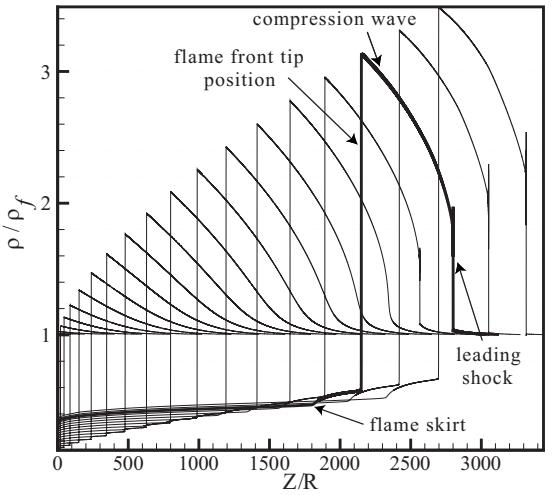

FIG. 7. Scaled density distribution along the channel axis for Re=6.67 at different time instants. Time instants are equally spaced in the range of $(0-3.8)U_f t/R$. The plot emphasized by bold corresponds to $U_f t/R=3.28$.

down the acceleration. In agreement with Eq. (8), absolute value of the negative velocity increases almost linearly with distance from the closed end of the tube. Velocity distribution along the tube axis ahead of the flame front is controlled mostly by the compression wave and by the shock dynamics. Flow velocity is not uniform in the transverse direction (along the x axis) either. Velocity profile over the tube cross-section is determined by the nonslip boundary conditions and by the regime of flame acceleration. The theory [20] predicted the velocity distribution in the incompressible exponential regime as

$$u_z=U_{axis}\frac{\cosh\sqrt{\sigma\,\mathrm{Re}}-\cosh(x\sqrt{\sigma\,\mathrm{Re}}/R)}{\cosh\sqrt{\sigma\,\mathrm{Re}}-1}. \tag{9}$$

In the stationary regime one should expect the Poiseuille velocity profile $u_z=U_{axis}(1-x^2/R^2)$. Figure 9 compares the

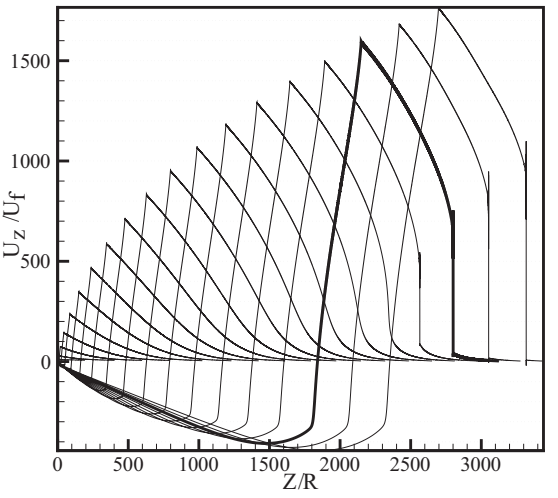

FIG. 8. Scaled velocity distribution along the channel axis for Re=6.67 at the same time instants as in Fig. 7.

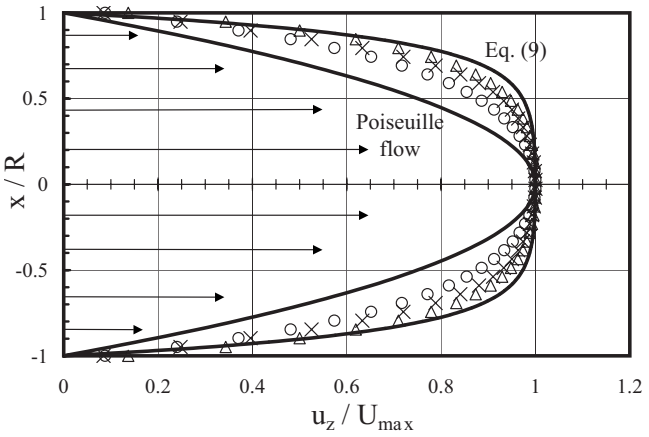

FIG. 9. The velocity profile u_z at the cross-section just ahead of the flame front scaled by the amplitude U_{max}. The solid lines shows the theoretical result Eq. (9) and the Poiseuille profile. The markers correspond to the simulation results for Re=6.67, at the time instants $U_f t/R=0.47;2.58;4.8$ (triangles, circles and crosses). The arrows illustrate the direction of the flow.

theoretical predictions to the numerical data at the time instants $U_f t/R=0.47;2.58;4.8$ (triangles, circles and crosses) corresponding to the exponential and linear regimes of flame acceleration, and to quasistationary supersonic burning. The theory [20] predicted the transitional layer ahead of an accelerating flame of the width about R/Θ. This width depends slightly on the Reynolds number of the flow, which makes a qualitative difference from the classical boundary layer produced by a stationary uniform flow. Figure 9 demonstrates that the theoretical estimates of [20] work quite well even at later stages of flame acceleration. Similar to the modeling of Ref. [20], the velocity profile in the exponential regime (Fig. 9, triangles) agrees quite well with the theory, Eq. (9). The velocity profile in the linear regime (circles) is an intermediate case between Eq. (9) and the Poiseuille profile. Surprisingly, the velocity profile in the stationary regime (crosses) is closer to Eq. (9) than to the Poiseuille flow. This effect may be understood from the three-dimensional (3D) representation of the flow velocity u_z shown in Fig. 10. The time instants $U_f t/R=0.7;3.12;3.94;4.71$ chosen in Fig. 10 correspond to the exponential regime of flame acceleration (a), to the linear regime before shock formation (b), to the linear regime after shock formation (c), and to the stationary supersonic flame propagation (d). Here, we can see dynamics of the compression wave and development of the shock. The shock front is almost planar, and it leads to the velocity jump, which is uniform in x direction just behind the shock. On the other hand, the boundary conditions require zero velocity at the walls. In that case one should expect relaxation of the gas velocity from the uniform flow to the Poiseuille flow at sufficiently large distances behind the shock. The expected velocity relaxation resembles the effect of the entry

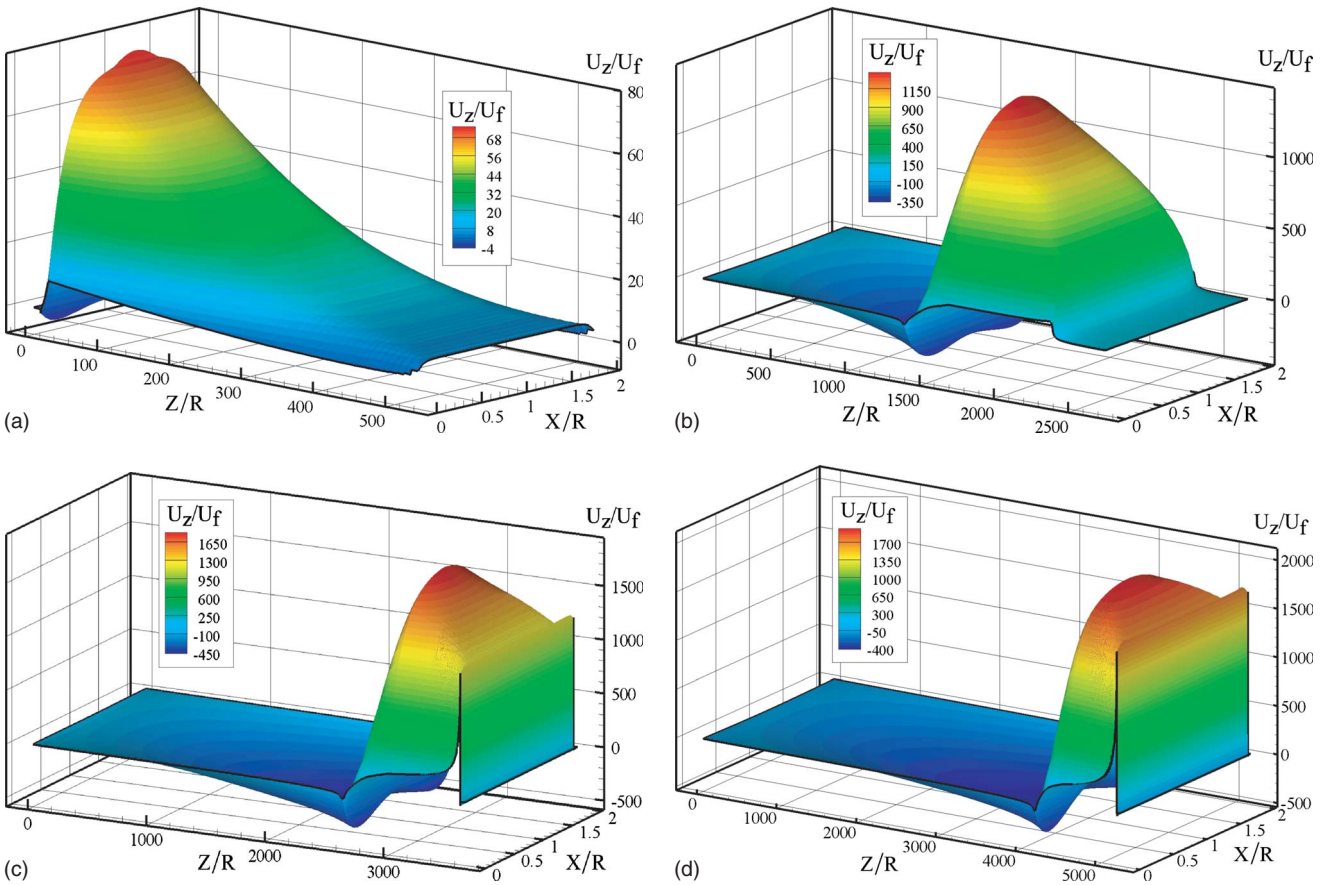

FIG. 10. (Color online) 3D representation of the flow velocity u_z for Re=6.67, at the time instants $U_f t/R=0.7;3.12;3.94;4.71$, figures (a), (b), (c), and (d), respectively.

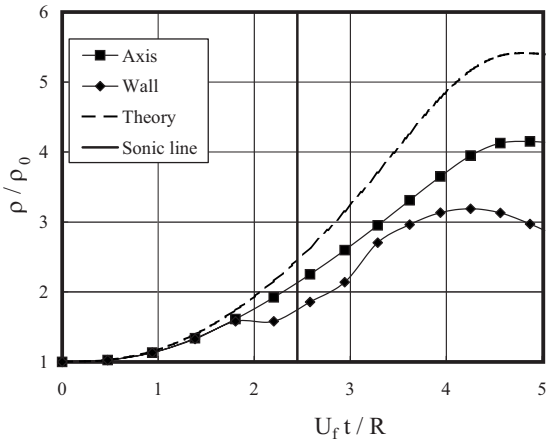

FIG. 11. Increase in the scaled density ρ/ρ_0 versus time just ahead of the flame front at the channel axis and at the walls. The dashed line presents the theoretical result Eq. (10).

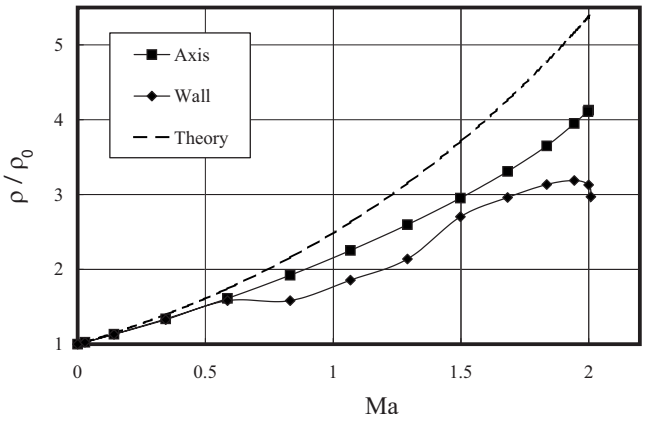

FIG. 12. Increase in the scaled density ρ/ρ_0 just ahead of the flame front at the channel axis and at the walls versus Mach number $\mathrm{Ma}_{tip}=U_{tip}/c_s$. The dashed line presents the theoretical result Eq. (10).

length of the Poiseuille flow in pipes and channels. Still, in the present case the distance available for the velocity relaxation is limited by the distance between the shock and the flame front. This distance is not sufficiently large for complete relaxation. The fuel mixture is consumed by the flame front before relaxation to the Poiseuille flow happens, and the velocity profile remains quite different from the Poiseuille one, see Fig. 9. Figure 10 illustrates also the negative compression flow in the burnt matter, which is minor in the plot (a) and quite strong in the plots (b)–(d).

Density and temperature of the fuel mixture ahead of the flame front become also nonuniform as local Mach number increases. Density variations along the channel axis are determined mostly by the spatial structure of the compression wave. Nonuniformity along the channel cross-section develops due to viscous heating. An interesting question in that context is the role of viscous heating and generation of entropy in the flow. The isentropic approximation is the basis for the classical theory of 1D compression flows [26]. The same approximation was used in [25] to describe detonation triggering by an accelerating flame. As long as the flow remains quasiplanar and quasi-isentropic, density in the fuel mixture increases because of the compression wave as [26]

$$\frac{\rho}{\rho_0}=\left(1+\frac{\gamma-1}{2}\frac{u}{c_s}\right)^{2/\gamma-1}. \tag{10}$$

The 1D theory may be compared to the simulation results substituting the flow velocity at the channel axis just ahead of the flame front into Eq. (10). Figure 11 shows density increase along the axis and at the walls versus time, as well as the predictions of the isentropic theory, Eq. (10). Figure 12 presents the same values versus the Mach number of the flame tip, $\mathrm{Ma}_{tip}=U_{tip}/c_s$. It is interesting that the isentropic relation Eq. (10) holds with a good accuracy at the channel axis up to the sonic point $\mathrm{Ma}_{tip}\approx 1$ and about, when the leading shock is rather weak. It is well-known that a shock produces entropy; a shock is the only source of entropy within the 1D theory without dissipations. Still, in the case of weak shocks, entropy jump scales as cube of the pressure jump, $\Delta S/S_0\propto(\Delta P/P_0)^3$, see [26], which makes weak shocks almost isentropic. In the present simulations the isentropic approach is violated noticeably earlier than a strong shock develops. Entropy in the flow is produced by viscous heating at the tube walls similar to the results of Ref. [24]. Paper [24] demonstrated both theoretically and numerically that viscous heating becomes important as the Mach number of the flow approaches unity. Figures 11 and 12 show that density at the wall is noticeably smaller than density at the axis. This happens because of additional heating of the fuel mixture at the walls due to the viscous stress. Additional heating and density decrease become especially strong in the late regime of stationary supersonic burning.

During the regime of almost constant acceleration, the flame passes the sound barrier, which is 10^3U_f in the present simulations, and propagates with supersonic velocity with respect to the tube walls, see Fig. 3. This does not contradict the general idea that flame (deflagration) is a subsonic combustion wave since flame velocity does remain subsonic with respect to the compressed fuel mixture. It is only the complex of flame-compression (shock) wave, which moves supersonically in the laboratory reference frame. The regime of almost constant flame acceleration is also limited in time. In our simulations we observed saturation of the flame tip velocity to the values about $2\cdot 10^3U_f=2c_s$. One should expect such an effect already from the basic theory [26], see also [27], since flame velocity cannot exceed the CJ deflagration speed. In the limit of large energy release $\Theta\gg 1$, the CJ deflagration speed in the laboratory reference frame may be evaluated as [27]

$$U_{CJ}=c_s\left[1+\frac{\gamma(\gamma-1)}{2(\gamma+1)}\right]\sqrt{2\frac{\Theta-1}{\gamma+1}}. \tag{11}$$

In the present case of $\Theta=8$, $\gamma=1.4$ this provides an evaluation $U_{CJ}\approx 2.68c_s$ for the CJ deflagration speed with respect to the tube walls. The saturation velocity of the flame tip observed in the present simulations is smaller, still, it is comparable to the CJ velocity. The difference between the classical theory and the present simulations is, presumably, due

to the nonslip boundary conditions at the walls, which produce viscous dissipations of the kinetic energy, a nonuniform velocity profile behind the shock and a strongly bend flame front. We remind that the classical theory [26] is limited to the 1D flow without losses, with uniform velocity and a planar flame. At the same time, the present numerical results are in a good agreement with the saturation velocity of "fast flames" observed experimentally in propane-air mixtures [10,28]. Using Eq. (11) with $\Theta=8$, $\gamma=1.4$ typical for propane-air flames, one should expect the CJ deflagration velocity with respect to the walls $U_{CJ}\approx 2.68c_s\approx 930$ m/s. The experiments [10,28] demonstrated a noticeably lower saturation velocity of the "fast flames" within the range of 600–750 m/s (one observes considerable scattering of the experimental data in [10,28]). These values are quite close to the present numerical data for the saturation velocity $2c_s \approx 700$ m/s. Still, one should take this agreement with caution keeping in mind considerable difference in the flow geometry of the present numerical study and the experiments [10,28].

Qualitatively, all regimes of flame acceleration found in the present work may be understood using the following simplified model. At the initial incompressible stage of the acceleration, flame dynamics is described by a differential equation

$$\frac{dU_{tip}}{dt}=\frac{U_f}{R}\sigma U_{tip}, \tag{12}$$

with σ determined by Eq. (7). As we discussed above, compression effects reduce the acceleration rate. Then, in the limit of small compression $\mathrm{Ma}\ll 1$, the differential equation for the tip velocity modifies as

$$\frac{dU_{tip}}{dt}=\frac{U_f}{R}\sigma U_{tip}\left[1-\alpha\mathrm{Ma}\frac{U_{tip}}{U_f}\right], \tag{13}$$

where α is some factor depending on the Reynolds number and on the expansion factor Θ. Equation (13) is Taylor expansion up to the first order in power of $\mathrm{Ma}\ll 1$. Solving Eq. (13), we find flame acceleration in the form

$$\frac{U_{tip}}{U_f}=\frac{\Theta\exp(\sigma U_f t/R)}{1+\alpha\mathrm{Ma}\Theta\exp(\sigma U_f t/R)}. \tag{14}$$

The solution Eq. (14) reproduces qualitatively all regimes of the flame acceleration found in our numerical simulations: initial exponential acceleration, asymptotic saturation to a stationary velocity $U_\infty=U_f/\alpha\mathrm{Ma}=c_s/\alpha$, and the transitional regime with an almost constant acceleration value $aR/U_f^2\approx\sigma/(4\alpha\mathrm{Ma})$. One is tempted to use a formula like Eq. (14) to describe the simulation results even quantitatively. In that case, we may use the saturation velocity value U_∞ from the simulations in order to determine the unknown factor α. Respective phenomenological plots for the flame velocity are shown in Fig. 3. Unfortunately, the phenomenological guess does not agree quantitatively with the simulation results, and a simple formula Eq. (14) provides only qualitative understanding of all regimes of flame acceleration.

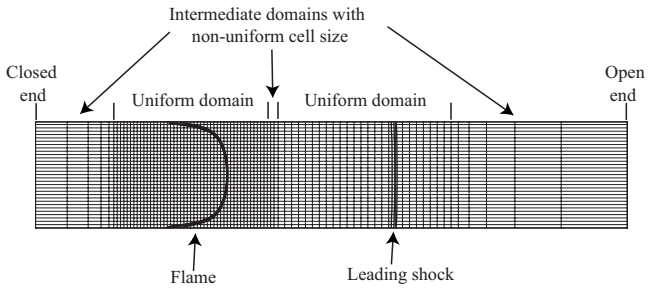

FIG. 13. The sketch of the grid with variable resolution used in numerical simulations.

IV. SUMMARY

In the Introduction, we pointed out a considerable gap, which was between the theoretical and/or numerical results [20,21] and the experimental data [9,10,23] on the flame acceleration in the DDT. There was also controversy between different numerical results on the subject [18–21,24]. This controversy happened because the numerical studies were rather fragmentary so far and/or of limited validity; they addressed different stages in the flame acceleration taken separately. In the present work we considered the whole process of flame acceleration in the DDT. We investigated systematically the flame acceleration in the extremely wide range of Mach numbers changing by 3 orders of magnitude. Flame accelerates from realistically small initial velocity with Mach number about 10^{-3} to supersonic speed in the reference frame of the tube walls. We show that flame acceleration undergoes three distinctive stages: (1) initial exponential acceleration in the quasi-isobaric regime similar to the previous works [20,21]; (2) linear increase in the flame velocity to supersonic speed with almost constant acceleration; (3) saturation to a stationary high-speed deflagration velocity. The saturation velocity may be correlated with the CJ deflagration speed; it is supersonic in the reference frame of the tube walls. Results on the exponential flame acceleration agree well with the previous theoretical and numerical studies

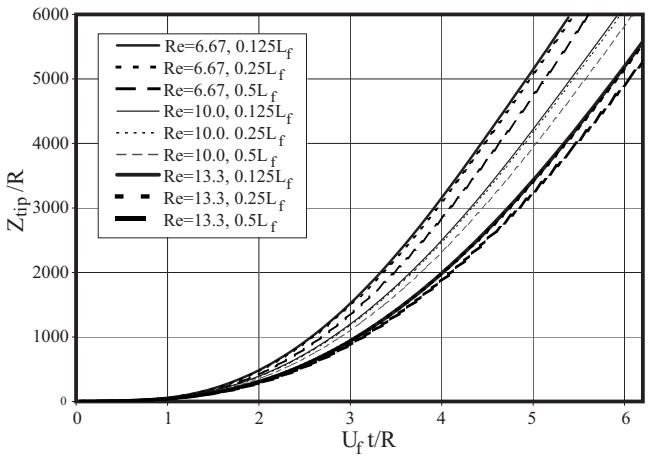

FIG. 14. Position of the flame tip versus time for different values of the mesh size and Reynolds number. Midthick lines correspond to Re=6.67, thin lines to Re=10.0, and thick lines to Re =13.3

TABLE I. Resolution tests for Re=6.67. Δz_f is the spatial step in the flame grid domain, $t_* U_f/R=4.8$ is the reference time moment after the end of flame acceleration (velocity saturation stage), Z_*/R and U_*/U_f are the flame tip position and saturation velocity, respectively, at the time moment t_*. $\Delta Z_*/R$ and $\Delta U_*/U_f$ are the increments of Z_*/R and U_*/U_f calculated in the table row i as $\Delta Z_*(i)=Z_*(i)-Z_*(i-1)$ and $\Delta U_*(i)=U_*(i)-U_*(i-1)$. Resolution in the wave grid domain $\Delta z_w=2\times\Delta z_f$ for each run.

$\Delta z_f/L_f$	Z_*/R	$\Delta Z_*/R$	U_*/U_f	$\Delta U_*/U_f$	$\Delta U_*/U_*$
0.5	4337.6		1982.9		
0.25	4660.9	323.3	2024.5	41.6	2.05%
0.125	4743.3	82.4	2028.9	4.4	0.22%

[20,21]. The saturation velocity is in line with previous experimental results [10,23,28]. Transition of flame acceleration regime from the exponential to the linear one, and then to the constant velocity, happens because of gas compression both ahead and behind the flame front.

An interesting question, which is not addressed in the present paper, concerns influence of heat loss to the walls on the DDT. Experiments [23] on the DDT in microscale tubes indicate that losses can bring a wider variety of different regimes in the DDT including stationary CJ deflagration without explosion and complete detonation failure. In the present work we do not consider losses, since careful study of these effects requires a paper as large as the present one. Investigation of the DDT in presence of losses is left for the future work.

ACKNOWLEDGMENTS

The authors are grateful to Leonid Kagan for useful discussions. This work has been supported by the Swedish Research Council (VR) and by the Kempe Foundation. Numerical simulations were performed at High Performance Computer Center North (HPC2N), Umeå, Sweden, within SNAC Project No. 007-07-25.

APPENDIX: NUMERICAL METHOD, RESOLUTION TESTS, AND NUMERICAL CHALLENGES

In our present simulations, we use a 2D planar hydrodynamic Eulerian code accounting for chemical reactions. The code is based on the cell-centered finite-volume scheme, which appears to be rather robust and accurate for modeling of different kinds of complex hydrodynamic flows [30–32]. The original code was developed for aeroacoustic applications, which are extremely critical in terms of accuracy, since both the turbulent flow and the resulting acoustic waves have to be captured. For example, the jet noise predictions [30,31] demonstrated very good results comparable with the best in the field. It was utilized successfully in studies of laminar and turbulent burning, hydrodynamic flame instabilities, flame acceleration, flame-sound interaction, and similar phenomena, e.g., see [17,16,20–22] and references therein. Present studies require that the code provides proper handling of shock waves and chemical fronts, which is crucial for reliable modeling of flame evolution and DDT.

The usual approach is to treat the convective flux approximations and the diffusive flux approximations separately because of different nature of these fluxes. For the convective fluxes we use a characteristic upwind flux scheme in which the propagation directions of the various characteristic variables are controlled by a user-given degree of up-winding. The numerical errors introduced by using this approximation are of the third order in the grid spacing assuming a smooth solution. Since in our problem most spatial scales are adequately resolved in the computational grid, we use an extremely small amount of upwinding, which gives us an almost fourth-order centered scheme with minimal numerical dissipation and dispersion. The numerical scheme is of the second order in space for diffusive terms; second-order accuracy in time is achieved by employing explicit Runge-Kutta temporal scheme. The total variation diminishing (TVD) limiter is applied in regions of high gradients to prevent overshoots in flow field properties for proper shock handling.

Multidimensional numerical simulation of flame acceleration and the DDT in a semi-infinite tube is a quite difficult

TABLE II. Resolution tests for Re=10.0. $t_* U_f/R=6.0$ is the reference time moment after the end of flame acceleration (velocity saturation stage), other notations are the same as in Table I. Resolution in the wave grid domain $\Delta z_w=2\times\Delta z_f$ for each run.

$\Delta z_f/L_f$	Z_*/R	$\Delta Z_*/R$	U_*/U_f	$\Delta U_*/U_f$	$\Delta U_*/U_*$
0.5	5821.8		1920.8		
0.25	6080.2	258.4	1930.1	9.3	0.48%
0.125	6139.6	59.4	1932.3	2.2	0.11%

TABLE III. Resolution tests for Re=13.3. $t_*U_f/R=6.9$ is the reference time moment after the end of flame acceleration (velocity saturation stage), other notations are the same as in Table I. Resolution in the wave grid domain $\Delta z_w=2\times\Delta z_f$ for each run.

$\Delta z_f/L_f$	Z_*/R	$\Delta Z_*/R$	U_*/U_f	$\Delta U_*/U_f$	$\Delta U_*/U_*$
0.5	6574.3		1868.3		
0.25	6909.8	335.5	1878.2	9.86	0.53%
0.125	6992.7	82.9	1880.8	2.63	0.14%

numerical task [33]. This problem involves a large range of different length and time scales related to the inner flame structure, to the elongated shape of the flame front, a large distance between the flame and the leading shocks, a thin layer of viscous heating close to the wall, fast development of the explosion, possibility of turbulence, interaction of shock waves and, finally, length and time scales related to detonation. All these scales require proper resolution in one simulation run. Particularly, we had to use the mesh with variable resolution in order to take into account the growing distances between the tube end, the accelerating flame and the shocks, and to resolve both chemical and hydrodynamic spatial scales. Typical computational resources for one such simulation required up to 5×10^3 processor hours, which required the use of parallel calculations.

We use a rectangular grid with the grid walls parallel to the coordinate axes. The sketch of the calculation grid is shown at Fig. 13. The tube length exceeds the tube radius significantly, reaching 1.2×10^4R at the end of the simulation runs. To perform all the calculations in a reasonable time, we made the grid spacing nonuniform along the z axis with the zones of fine grid around the flame and leading shock fronts. In the flame and shock wave domains the grid size in z direction was, correspondingly, $0.25L_f$ and $0.5L_f$ for main calculation runs, which allowed us to resolve the internal structure of the flame and shock waves, e.g., see our previous tests in [34]. Outside the region of fine grid the cell size grows gradually with $\approx2\%$ change in size between the neighboring cells. In order to keep the flame and shock waves in the zone of fine grid we implemented the periodical mesh reconstruction during the calculation run. Splines of the third order are used for reinterpolation of the flow variables during periodic grid reconstruction. Along the x axis we used a uniform grid, which allowed us to resolve quite well the zone of large velocity gradients close to the walls.

In order to check if the used resolution is sufficient, we performed the resolution tests for Re=6.67,10.0,13.3. For all cases, the grid size in flame domain varied between $0.125L_f$, $0.25L_f$, and $0.5L_f$. We checked the position and velocity of the flame tip at particular chosen time instants $t_*U_f/R=4.80,6.0,6.9$ for Re=6.67,10.0,13.3, respectively, corresponding to the stage of flame velocity saturation. The resolution test results are presented in Table I (Re=6.67), Table II (Re=10.0), Table III (Re=13.3), and Fig. 14. Both the tables and the figure show good convergence of the numerical solution at the flame acceleration and saturation stages.

As one can see from the Figs. 7 and 8, there are small numerical oscillations of density and velocity at the leading shock wave front, which are not totally eliminated by the applied TVD-limiting. In order to check if these oscillations can affect the saturation flame velocity, we performed an additional set of resolution tests for the leading shock wave domain, which is presented in the Table IV. We took initial Mach number Ma=0.01 in order to obtain saturation velocity faster. The resolution tests show that by increasing the wave domain resolution we obtain only minor changes in the saturation velocity, and the resolution values employed in main simulation runs are adequate. In runs of Table IV the resolution in flame domain is kept constant, while in runs of Tables I–III resolution values in flame and shock wave domains change together. Comparison of relative change in saturation velocity $\Delta U_*/U_*$ for all resolution tests in Tables I–IV shows that resolution in shock wave domain has smaller influence on saturation velocity than that in flame domain.

The main conclusion of the tests is that the used resolution allows to capture quite well all important features of flame acceleration investigated in this paper.

In the present work the quantitative studies are concentrated on the first part of the DDT process, namely, on the

TABLE IV. Resolution tests for shock wave domain, Re=6.67, flame domain resolution $\Delta z_f/L_f=0.5$, initial Mach number Ma=0.01. Δz_w is the spatial step in the wave grid domain, $t_*U_f/R=4.8$ is the reference time moment after the end of flame acceleration (velocity saturation stage), other notations are the same as in Table I.

$\Delta z_w/L_f$	Z_*/R	$\Delta Z_*/R$	U_*/U_f	$\Delta U_*/U_f$	$\Delta U_*/U_*$
1.0	562.36		201.19		
0.5	569.28	6.92	201.56	0.37	0.18%
0.25	572.05	2.77	201.69	0.13	0.06%
0.125	572.22	0.17	201.73	0.04	0.02%

flame acceleration and velocity saturation. The flow remains laminar in the whole range of flame acceleration, which is covered by the resolution tests. Particularly, for Re=6.67, convergence is demonstrated up to the scaled time instant $U_f t/R=4.8$, for Re=10.0 up to the scaled time instant $U_f t/R=6.0$, for Re=13.3 up to the scaled time instant $U_f t/R=6.9$. At later time moments the process of explosion starts gradually.

[1] Ya. B. Zeldovich, G. I. Barenblatt, V. B. Librovich, and G. M. Makhviladze, *Mathematical Theory of Combustion and Explosion* (Consultants Bureau, New York, 1985).

[2] K. I. Shelkin, Zh. Eksp. Teor. Fiz. **10**, 823 (1940).

[3] P. A. Urtiew and A. K. Oppenheim, Proc. R. Soc. London, Ser. A **295**, 13 (1966).

[4] J. E. Shepherd and J. H. S. Lee, *Major Research Topics in Combustion* (Springer-Verlag, Hampton, VA, 1992).

[5] S. Kerampran, D. Desbordes, and B. Veyssiere, Combust. Sci. Technol. **158**, 71 (2000).

[6] M. Cooper, S. Jackson, J. M. Austin, E. Wintenberger, and J. E. Shepherd, AIAA Paper No. 2001-3812 (2001).

[7] G. D. Roy, S. M. Frolov, A. A. Borisov, and D. W. Netzer, Prog. Energy Combust. Sci. **30**, 545 (2004).

[8] G. Ciccarelli, C. Fowler, and M. Bardon, Shock Waves **14**, 161 (2005).

[9] M. Kuznetsov, V. Alekseev, I. Matsukov, and S. Dorofeev, Shock Waves **14**, 205 (2005).

[10] G. Ciccarelli and S. Dorofeev, Prog. Energy Combust. Sci. **34**, 499 (2008).

[11] B. Hof, C. W. H. van Doorne, J. Westerweel, and F. T. M. Nieuwstadt, Phys. Rev. Lett. **95**, 214502 (2005).

[12] D. Sundkvist, V. Krasnoselskikh, P. K. Shukla, A. Vaivads, M. Andre, S. Buchert, and H. Reme, Nature (London) **436**, 825 (2005).

[13] G. Searby and P. Clavin, Combust. Sci. Technol. **46**, 167 (1986).

[14] A. R. Kerstein, W. T. Ashurst, and F. A. Williams, Phys. Rev. A **37**, 2728 (1988).

[15] V. Bychkov, Phys. Rev. E **68**, 066304 (2003).

[16] V. Akkerman, V. Bychkov, and L. E. Eriksson, Combust. Flame **151**, 452 (2007).

[17] V. Akkerman, V. Bychkov, L. de Goey, R. Bastiaans, J. van Oijen, and L.-E. Eriksson, Phys. Fluids **20**, 055107 (2008).

[18] L. Kagan and G. Sivashinsky, Combust. Flame **134**, 389 (2003).

[19] J. D. Ott, E. S. Oran, and J. D. Anderson, AIAA J. **41**, 1391 (2003).

[20] V. Bychkov, A. Petchenko, V. Akkerman, and L.-E. Eriksson, Phys. Rev. E **72**, 046307 (2005).

[21] V. Akkerman, V. Bychkov, A. Petchenko, and L.-E. Eriksson, Combust. Flame **145**, 206 (2006).

[22] V. Bychkov, V. Akkerman, G. Fru, A. Petchenko, and L. E. Eriksson, Combust. Flame **150**, 263 (2007).

[23] M. Wu, M. Burke, S. Son, and R. Yetter, Proc. Combust. Inst. **31**, 2429 (2007).

[24] D. Valiev, V. Bychkov, V. Akkerman, and L.-E. Eriksson, Phys. Lett. A **372**, 4850 (2008).

[25] V. Bychkov and V. Akkerman, Phys. Rev. E **73**, 066305 (2006).

[26] L. D. Landau and E. M. Lifshitz, *Fluid Mechanics* (Pergamon Press, Oxford, 1989).

[27] R. Chue, J. Clarke, and J. H. Lee, Proc. R. Soc. London, Ser. A **441**, 607 (1993).

[28] M. Kuznetsov, V. Alekseev, Yu. Yankin, and S. Dorofeev, Combust. Sci. Technol. **174**, 157 (2002).

[29] V. Bychkov, D. Valiev, and L.-E. Eriksson, Phys. Rev. Lett. **101**, 164501 (2008).

[30] N. Andersson, L.-E. Eriksson, and L. Davidsson, Int. J. Heat Fluid Flow **26**, 393 (2005).

[31] N. Andersson, L.-E. Eriksson, and L. Davidsson, AIAA J. **43**, 1899 (2005).

[32] C. Wollblad, L. Davidson, and L.-E. Eriksson, AIAA J. **44**, 2340 (2006).

[33] V. Gamezo, T. Ogawa, and E. Oran, Combust. Flame **155**, 302 (2008).

[34] V. Akkerman, V. Bychkov, A. Petchenko, and L.-E. Eriksson, Combust. Flame **145**, 675 (2006).